Surface Plasmon Resonance Imaging Measurements of Ultrathin Organic Films

Jennifer M. Brockman, Bryce P. Nelson, and Robert M. Corn

Department of Chemistry, University of Wisconsin-Madison, Madison, Wisconsin 53706-1396; e-mail: brockman@corninfo.chem.wisc.edu, nelsonb@corninfo.chem.wisc.edu, corn@chem.wisc.edu

Key Words   microscopy, Fresnel calculations, self-assembled monolayers, DNA arrays, protein-DNA interactions

■ **Abstract**   The surface-sensitive optical technique of surface plasmon resonance (SPR) imaging is used to characterize ultrathin organic and biopolymer films at metal interfaces in a spatially resolved manner. Because of its high surface sensitivity and its ability to measure in real time the interaction of unlabeled biological molecules with arrays of surface-bound species, SPR imaging has the potential to become a powerful tool in biomolecular investigations. Recently, SPR imaging has been successfully implemented in the characterization of supported lipid bilayer films, the monitoring of antibody-antigen interactions at surfaces, and the study of DNA hybridization adsorption. The following is included in this review: (*a*) an introduction to the principles of surface plasmon resonance, (*b*) the details of SPR imaging instrumental design, (*c*) a short discussion concerning resolution, sensitivity, and quantitation in SPR imaging, (*d*) the details of DNA array fabrication on chemically modified gold surfaces, and (*e*) two examples that demonstrate the application of the SPR imaging technique to the study of protein-DNA interactions.

INTRODUCTION

Surface plasmon resonance (SPR) reflectivity measurements are surface-sensitive, spectroscopic methods that can be used to characterize the thickness and/or index of refraction of ultrathin organic and biopolymer films at noble metal (Au, Ag, Cu) surfaces. Since the introduction of the BIAcore® SPR instrument (1, 2), SPR spectroscopy has become widely used in the fields of chemistry and biochemistry to characterize biological surfaces and to monitor binding events. The success of these SPR measurements is primarily due to three factors: (*a*) With SPR spectroscopy, the kinetics of biomolecular interactions can be measured in real time, (*b*) the adsorption of unlabeled analyte molecules to the surface can be monitored, and (*c*) SPR has a high degree of surface sensitivity that allows weakly bound interactions
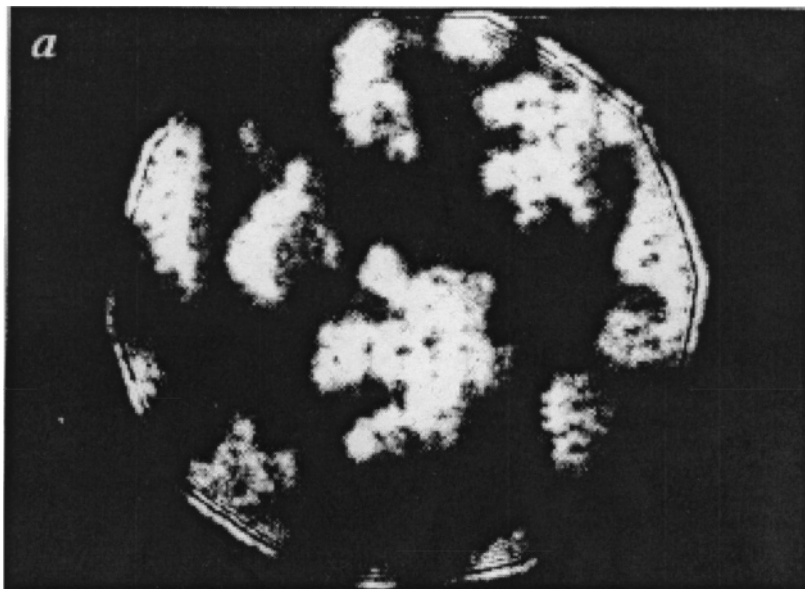
Figure 1 Surface plasmon resonance image of a DMPA (dimyristoylphosphatidic acid) monolayer transferred to a gold solid support. The film was transferred at a lateral pressure where condensed and expanded domains coexist; the condensed phases appear as the light regions in the image. (Reprinted with permission from Reference 17.)

to be monitored in the presence of excess solution species. SPR spectroscopy has been used to monitor such events as antibody-antigen binding (3, 4), DNA hybridization (5–7), and protein-DNA interactions (8–11). [For other recent reviews, see Silin & Plant (12), Fivash et al (13), and http://www.biacore.com/scientific/index.html].

The technique of SPR imaging (also denoted as SPR microscopy) couples the sensitivity of scanning angle SPR measurements with the spatial capabilities of imaging. Shortly after its invention (14–16), SPR microscopy was first used in a biomolecular application for the imaging of phospholipid monolayer films (17). In Figure 1, a SPR image reprinted from this pioneering work is shown. A monolayer film of dimyristoylphosphatidic acid was transferred to a gold-coated solid support at a lateral pressure where condensed and expanded domains coexist; the light areas correspond to condensed lipid domains and the dark areas correspond to expanded lipid domains. Since these initial efforts, SPR imaging has also been used for surface morphological investigations of many surface systems, including self-assembled monolayer films (18, 19), mono- and multilayer films prepared by Langmuir Blodgett techniques (20, 21), and multilayer films built by alternate polyelectrolyte deposition (22, 23).

Because SPR imaging can monitor the amount and distribution of molecules adsorbing onto a metal surface in real time and with a relatively high degree of

lateral resolution, it is an ideal way to monitor the binding of molecules onto arrays of surface-bound species. Multiple interactions can be screened simultaneously with SPR array measurements under exactly the same adsorption conditions, and control measurements can be built in to consider such factors as nonspecific binding. Data collected with such an array format saves time and reduces the amount of sample required, which is especially important in biological systems. Recently, SPR imaging has been used in this array-type manner to study antibody-antigen (24, 25), DNA-DNA (26–28), and DNA-protein (23, 29) interactions.

The aim of this review is to familiarize the reader with the technique of SPR imaging, to discuss the application of the technique to the study of ultrathin organic and biopolymer films, and to present recent results generated in our laboratory that employ SPR imaging in the study of protein-DNA interactions. The paper is organized as follows: In the first section, a short introduction to the theory behind surface plasmon generation is provided. Fresnel reflectivity contour plots are then utilized to explain several methods of SPR measurement, including SPR imaging. In the second and third sections, the specifics of SPR imaging instrumental design are discussed and such factors as resolution, sensitivity, and quantitation are considered. In the fourth section, an overview of sample preparation is given and the specific surface attachment chemistries used in our laboratory to construct biomolecular arrays used in SPR imaging experiments are discussed. In the final section, some recent applications of SPR imaging are reviewed and data from ongoing experiments in our laboratory, which utilize the technique to monitor the sequence specific binding of proteins to arrays of surface-bound DNA, are presented.

THEORY

Surface plasmons (SPs), also known as surface plasmon polaritons, are surface electromagnetic waves that propagate parallel to a metal/dielectric interface. For SPs to exist at such an interface, the real part of the dielectric constant $Re(\varepsilon)$ of the two media must be of opposite sign. This condition is met in the infrared (IR)-visible region for air/metal and water/metal interfaces (where the ε of metals is negative and that of air or water is positive). Typically, Au and Ag are used in SPR experiments, but metals such as Cu, Ti, or Cr can also support SP generation. SPs have been used to enhance the sensitivity of several spectroscopic measurements, including fluorescence (30, 31), Raman scattering (31–34), and optical second harmonic generation (35, 36). However, in their simplest form, SPs can be used to probe changes in the index of refraction or thickness of ultrathin organic films adsorbed at metal surfaces using SPR reflectivity measurements.

SPs are created when the light energy from p-polarized incident photons is coupled into oscillating modes of free electron density present in the metal film. The SPs are evanescent waves that have their maximum intensity at the interface

and decay exponentially away from the phase boundary to a penetration depth on the order of 200 nm. SPs cannot be excited directly at planar air/metal or water/metal interfaces because momentum-matching conditions cannot be satisfied. [For a more detailed discussion, see Hanken et al (37) and Knoll (38).] Therefore, it becomes necessary to use a prism-coupling arrangement or a grating to excite SPs (38). The most commonly used setup in SPR imaging experiments is attentuated total reflectance prism coupling in the Kretschmann configuration. Here, a thin metal layer (∼50 nm thick) is placed in direct contact with a prism. In this arrangement, the evanescent light wave produced at the prism/air or prism/metal interface during total internal reflection is used to excite SP modes at the metal surface.
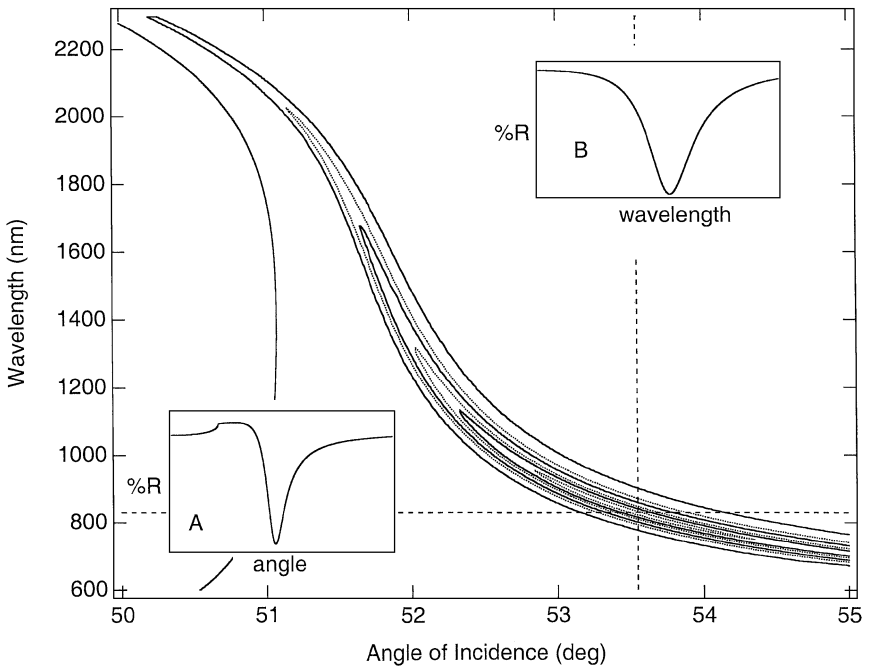
Fresnel Reflectivity Calculation Contour Plots

Three-dimensional reflectivity contours such as those shown in Figure 2 can be used to describe the variation in SPR reflectivity as a function of both wavelength and angle of incidence. These contours are generated using complex, three-phase Fresnel calculations that model the percent reflectivity (%R) as a function of wavelength and incident angle for a prism/gold film/water three-phase system. (For the specific contour plot shown in Figure 2, the prism was assumed to be composed of SF-10 glass and the thickness of the gold layer was set to 45.0 nm.) Each contour line represents a region of constant reflectivity; contours from 1%–50% reflectivity are shown in Figure 2. The Fresnel calculations used to construct the contour plot were performed using an N-phase method outlined by Hansen (39); they factor in the dispersion of the prism (40), gold (41), and water (42). Details concerning our specific implementation of these calculations are outlined in depth elsewhere (43; see also http://corninfo.chem.wisc.edu/calculations.html).

Methods of Measurement

Commonly, SPR measurements are collected in one of three modes: (*a*) scanning angle SPR (also denoted as SPR angle shift), (*b*) SPR wavelength shift, and (*c*) SPR imaging. The most widely employed method, the scanning angle SPR measurement, uses a single wavelength for excitation and measures the %R from a prism/gold film assembly as a function of incident angle. A theoretical SPR reflectivity versus angle curve can be generated from the contour plot shown in Figure 2 by taking a cut parallel to the x-axis. As the incident angle increases from <50° to ∼51°, the critical angle is reached, total internal reflection occurs, and the reflected intensity at the interface is nearly 100%. As the angle increases further, SPs are created at the prism/gold interface and the reflected intensity is therefore damped. A minimum in the reflected light intensity from this bare gold surface occurs at an angle of ∼53.7°; this angle is referred to as the SPR angle. The position of the SPR angle is sensitive to changes in the index of refraction at or very near the surface; this includes changes in the thickness and/or index of refraction of any adsorbed material at the metal surface. The dotted line in

Figure 3*a* shows a theoretical SPR curve for the same gold surface after the adsorption of a 5.0 nm film ($n = 1.45$). Apparent in Figure 3 is the shift in the location of the SPR minimum. Quantitation of this SPR angle shift is the basis for most SPR adsorption sensors, including the commercially available BIAcore instrument.

Most commonly, a low-power HeNe laser (632.8 nm) is used for such scanning angle measurements, but other wavelengths can also be employed. A two-color approach developed by Peterlinz et al (7, 44) utilizes HeNe lines at both 632.8 and 543.5 nm to determine both the thickness and the dielectric constant of an adsorbing thin film unambiguously. In addition, we recently reported the use of near-IR (NIR) wavelengths for scanning angle measurements (23), and others have used NIR and

Figure 2 Surface plasmon resonance (SPR) reflectivity contour plot. These contours were generated from three-phase complex Fresnel calculations for a SF-10/Au/water system (gold thickness 45.0 nm). Regions of constant reflectivity (1%, 5%, 10%, 20%, 30%, and 50%) are plotted as a function of wavelength and angle of incidence. The *solid dark line* in the *left* side of the figure shows the wavelength dependence of the critical angle. A reflectivity versus angle curve can be generated from the contour plot by cutting parallel to the x-axis (*inset, lower left*) [the cut shown corresponds to 830-nm excitation (for the SPR curve corresponding to this cut, see Figure 3*A*)] and a reflectivity versus wavelength curve by cutting parallel to the y-axis (*inset, upper right*). The 45.0-nm gold thickness is optimal for excitation from 750 to 950 nm.
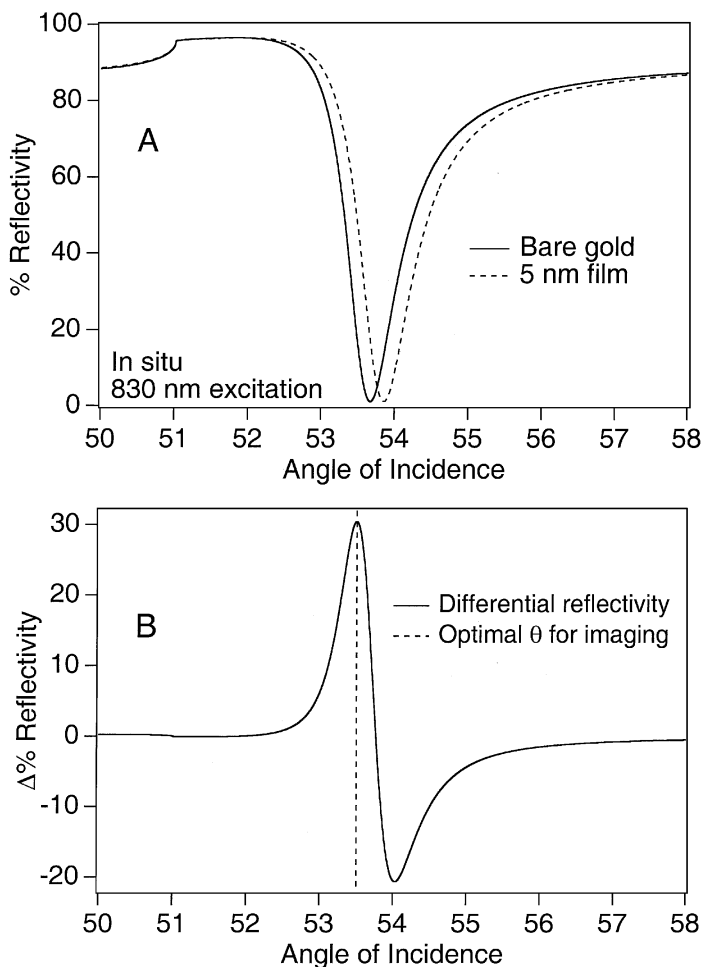
Figure 3   (*A*) Calculated surface plasmon resonance (SPR) curves at 830-nm excitation for (*solid line*) a three-layer system composed of an SF-10 glass prism ($n = 1.711$), a 45.0-nm-thick Au film ($n = 0.165 + 5.205i$), and an infinite layer of water ($n = 1.327$) and (*dashed line*) a four-layer system composed of an SF-10 glass prism ($n = 1.711$), a 45.0-nm-thick Au film ($n = 0.165 + 5.205i$), a 5.0-nm-thick biopolymer film ($n = 1.45$), and an infinite layer of water ($n = 1.327$). (*B*) A differential SPR reflectivity curve obtained by subtracting the two curves shown in *A*. The *dotted line* indicates the optimal angle setting for SPR imaging measurements.

IR wavelengths as well (45–49). Despite the significant increase in wavelength, measurements in the NIR have sensitivities equal to those performed in the visible region and can be advantageous in two respects. First, NIR excitation produces smaller angle shifts and sharper minima, which increases the practical dynamic range of the technique, allowing for the measurement of thicker films. Second, NIR wavelengths can be used to measure films that contain species that absorb light in the visible region of the spectrum.

An alternative method for performing the SPR experiment is to sit at a fixed incident angle and measure reflectivity as a function of wavelength. A theoretical SPR reflectivity versus wavelength curve can be generated from the contour plot shown in Figure 2 by taking a cut parallel to the y-axis. In this case, a minimum in reflectivity occurs at a certain wavelength, and the position of this minimum shifts upon adsorption of material at the interface. Typically, films with minima at wavelengths from 600 to 800 nm are employed in these SPR wavelength shift measurements (50–57), but recent work in our laboratory has demonstrated that a Fourier transform spectrometer can be used to perform SPR wavelength shift measurements in the near IR region from 12000 to 6000 cm^{-1} (58).

In an SPR imaging experiment, spatial differences in %R (due to differences in film thickness or index of refraction across the metal surface) are measured at a fixed angle. A collimated, monochromatic beam of light is used to illuminate the sample assembly at a single incident angle (near the SPR angle), and the light reflected from the surface is detected with an inexpensive charge coupled device (CCD) camera to produce the SPR image. Consider the bare gold/5.0-nm biopolymer film system described earlier. The theoretical SPR curves calculated for these two films are shown in Figure 3A. Note again the shift in the SPR angle due to the increased film thickness on polymer adsorption. Now imagine a dual-component surface containing regions of both bare gold and a 5.0-nm-thick polymer film. Subtraction of the two SPR curves in Figure 3a results in the differential reflectivity curve shown in Figure 3B. The maximum and minimum values represent the angles of maximum contrast for the two-component surface and are hence the optimal angles at which to collect data in a SPR imaging experiment. At the angle corresponding to the maximum differential, %R, the polymer regions will appear light against a dark background, and at the angle corresponding to the minimum differential %R, the image contrast will be reversed. Although either angle is suitable for imaging this two-component substrate, it is advantageous to perform experiments at the smaller incident angle if additional adsorption events are to be monitored. This prevents crossover of the image contrast, as the films become increasingly thick.

INSTRUMENTATION

A schematic diagram of the SPR imaging apparatus is shown in Figure 4. A collimated, polychromatic light source passes through a polarizer and impinges on a prism/thin gold film sample assembly at an angle near the SPR angle. The
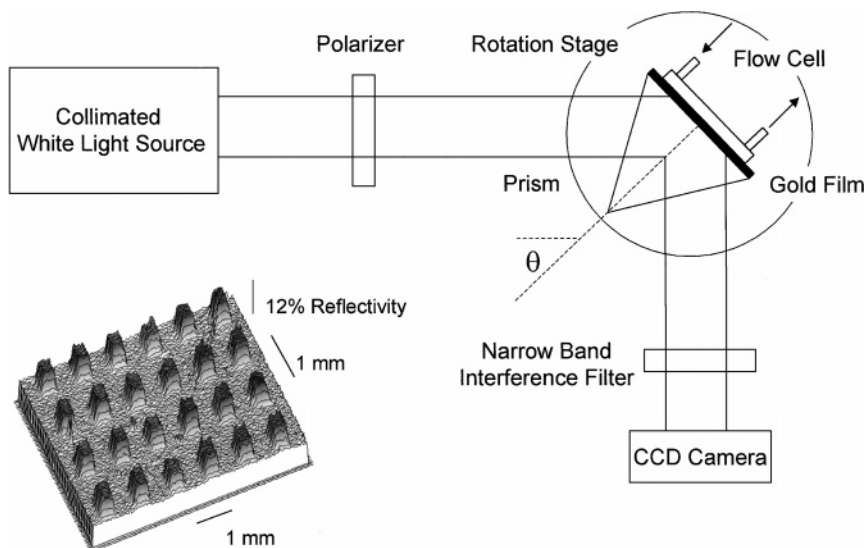
Figure 4 Surface plasmon resonance (SPR) imaging experimental setup. Light from a collimated polychromatic source passes through a polarizer and impinges on a prism/Au sample assembly at a specific angle of incidence, θ, near the SPR angle. The reflected light passes through a narrow-band interference filter and is detected with an inexpensive CCD camera. The prism/Au sample assembly is mounted on a rotation stage so that θ can be manipulated, and a liquid flow cell is attached to the assembly permitting in situ adsorption measurements. An image of a 24-spot oligonucleotide array onto which DNA single-stranded binding protein has bound is shown in the *lower left*.

reflected light then passes through a narrow-band interference filter and is detected with an inexpensive CCD camera. The prism/thin gold film sample assembly is mounted on a rotation stage so that the incident angle can be manipulated; this allows for ease in maximizing the contrast of the SPR image. A liquid flow cell is attached to the assembly, permitting images to be collected in situ. Simple removal of this cell attachment allows for the collection of images ex situ.

Commonly, the light source used in SPR imaging experiments consists of a single wavelength laser beam that has been expanded and collimated with appropriate optics. However, we have recently replaced this source with a collimated white light/narrow-band NIR interference filter combination (23). Three distinct advantages result from this experimental configuration: (*a*) The sharpness of the SPR resonance in the NIR leads to larger reflectivity changes on adsorption, (*b*) the excitation wavelength can be easily varied by changing filters and images can be collected at multiple wavelengths, and (*c*) the incoherence of the white light source eliminates interference fringes that are often problematic when using coherent laser excitation. These various advantages greatly improve both quality and sensitivity of the imaging measurement. In a variation of the white

light imaging experiment, Knobloch et al (59) used broadband excitation from an incoherent source to collect SPR images. For a given incident angle and a given film thickness/index of refraction, a narrow spectral band of the incident light was at resonance. Therefore, features with different thicknesses appeared as different colors in images recorded with a color camera.

RESOLUTION, SENSITIVITY, AND QUANTITATION

The propagation length, L_x, of the SPs limits the lateral resolution of SPR imaging. (In order to be resolved, two neighboring areas on a sample surface must each be approximately L_x in size.) This propagation length varies greatly for different metals and for different wavelengths used in the imaging experiment. On gold surfaces, the propagation length decreases as the SP excitation wavelength decreases. For example, at a wavelength of 676.4 nm, the plasmon propagation length for a 44-nm-thick gold film is calculated to be 14 μm, whereas a L_x of 0.5 μm is calculated for a wavelength of 530.9 nm. Figure 5 shows an SiO$_2$ test pattern on gold that was imaged with five different wavelengths, ranging from 676.4 nm to 530.9 nm (60). The increase in resolution as the excitation wavelength decreases is apparent.

As stated above, collecting SPR measurements using NIR wavelengths has the advantages that it allows for the measurement of thicker films and enables the measurement of films that absorb appreciably in the visible region. As also

676.4 nm   647.1 nm   632.8 nm   568.2 nm   530.9 nm
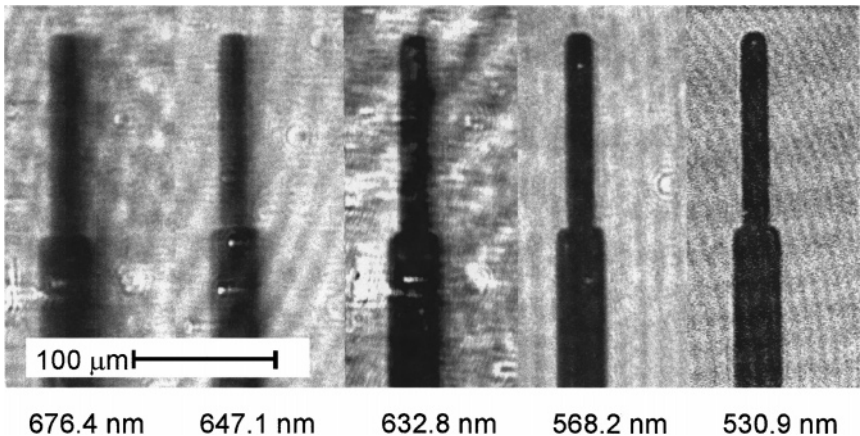
Figure 5 An SiO$_2$ test pattern on gold, imaged with five different wavelengths: 676.4, 647.1, 632.8, 568.2, and 530.9 nm, respectively. Correction using p- and s-polarized light was applied. The plasmon vector is pointing to the *right*, and the *dark area* is the bare gold at resonance. The contrast of the images was chosen such that the grey value range was used in an optimal way. (Reprinted with permission from Reference 60.)

mentioned, in the SPR imaging experiments, NIR excitation has the additional advantage that these longer wavelengths produce images with higher contrast than do wavelengths in the visible region (60, 61). However, the advantages gained by moving to longer excitation wavelengths are coupled with a measurable loss in the lateral resolution. Hence, the wavelength at which to conduct the SPR imaging experiment must be optimized so as to obtain the highest level of contrast possible while still maintaining sufficient lateral resolution. In our laboratory, excitation wavelengths ranging from 800 to 1000 nm are employed, providing lateral resolutions on the order of 25 μm.

SPR imaging has sufficient sensitivity to determine film thickness with near-Angstrom-level resolution (16, 20, 62). Although the sensitivity of SPR imaging cannot match that of fluorescence microscopy experiments, it has the advantage that it does not require the presence of labeled molecules. In addition, the surface selectivity of the SPR measurement is such that it can be performed in the presence of a substantial solution population of adsorbing molecules. (In fluorescence imaging, a rinsing step is required in order to reduce the strong background fluorescence from tagged molecules present in solution.) As a result, weaker surface interactions (e.g. protein-DNA binding) can be studied with the SPR imaging method.

Quantitative measurements of biomolecule adsorption can be accomplished using SPR imaging techniques. For example, Zizlsperger & Knoll (63) used SPR microscopy combined with image analysis software to measure the binding of streptavidin to surface-immobilized biotinylated alkanethiols. Here, the sample and camera positions were rotated step-wise, images were collected at multiple angles, and analysis software was used to construct SPR curves for an array of discreet surface locations. The optical thickness of the material at each array location could then be calculated precisely using Fresnel equations. However, real-time measurements (and hence kinetic data) cannot be collected in this fashion. For kinetic measurements, images are acquired at a fixed angle in a time-dependent manner. The time resolution depends on the transfer time of the camera and frame-grabber card used in the experiment; resolutions from ∼600 to 1000 ms have been reported (63). The series of images are then deconstructed, and Fresnel calculations based on changes in reflectivity are used to determine the thickness/amount of bound material.

SURFACE CHEMISTRY AND ARRAY FABRICATION

The immense power of SPR imaging stems from its ability to monitor the binding of analytes to arrays of bound species simultaneously, saving time and sample, and rendering more accurate results. In our laboratory, we are especially interested in creating multicomponent oligonucleotide arrays to use in the monitoring of protein-DNA interactions with SPR imaging. To this end, we have developed a fabrication procedure that makes use of reversible protecting groups to manipulate surface properties during array construction (29, 64). To spatially confine aqueous

solutions of each different DNA sequence during immobilization, the surface must be initially hydrophobic. However, once the oligonucleotide sequences have been attached, it is necessary that the array background be resistant to the nonspecific binding of analyte proteins. The array fabrication procedure is depicted schematically in Figure 6 and proceeds as follows:
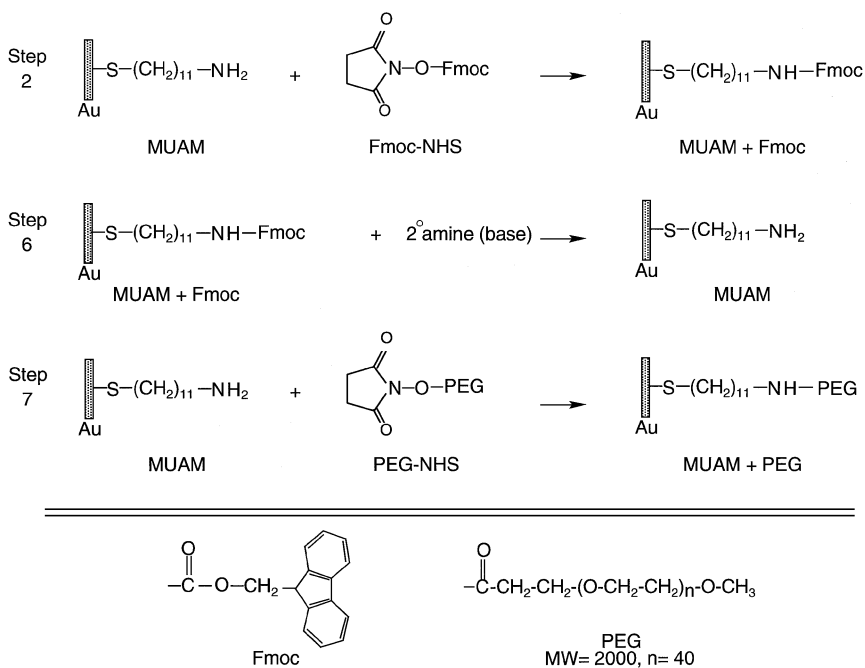
1. A monolayer of 11-mercaptoundecylamine (MUAM) is adsorbed via self-assembly onto an evaporated gold thin film.
2. The MUAM-modified gold surface is then reacted with a reversible amine 9-fluorenylmethoxycarbonyl (Fmoc) protecting group (65) to form a
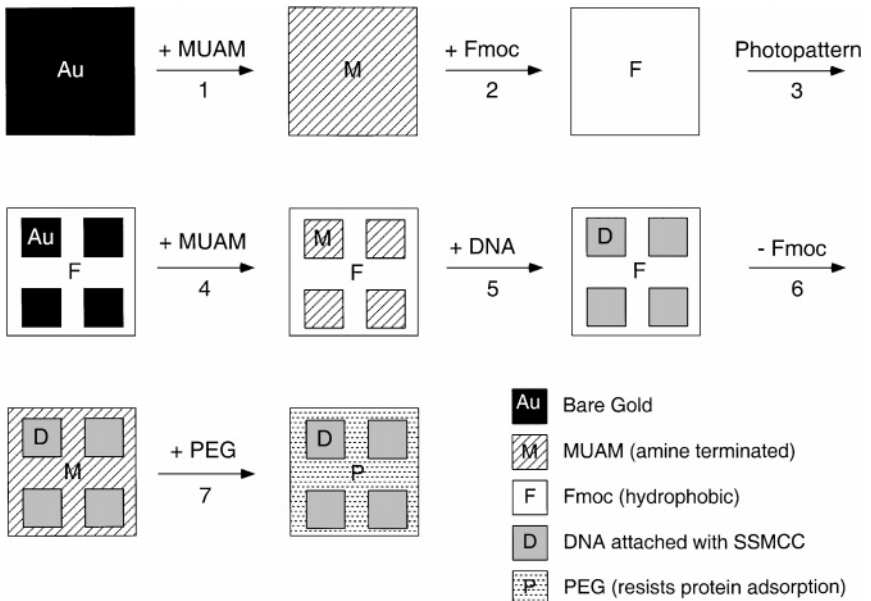

Figure 6   Modification procedure used for the construction of multicomponent DNA arrays. A clean gold surface is reacted with 11-mercaptoundecylamine (MUAM) (an amine-terminated alkanethiol) and subsequently reacted with the *N*-hydroxysuccinimide ester of Fmoc (Fmoc-NHS) to form a hydrophobic surface. The surface is then exposed to ultraviolet radiation through a quartz mask and rinsed with solvent to remove the MUAM + Fmoc from selected areas on the surface, leaving bare gold pads. The bare gold pads are then filled in with MUAM, which results in an array of reactive MUAM pads surrounded by a hydrophobic, Fmoc-terminated background. DNA solutions are then spotted onto specific array locations by pipette, where the molecules become covalently bound to the surface via the bifunctional linker sulfosuccinimidyl 4-(*N*-maleimidomethyl)cyclohexane-1-carboxylate (SSMCC). In the final two steps, the Fmoc groups are removed and replaced by methoxypoly(ethylene glycol) propionic acid (PEG) groups, which help to inhibit the nonspecific adsorption of analyte proteins to the array background. (Reprinted with permission from Reference 29.)

hydrophobic surface. Specifically, the *N*-hydroxysuccinimide ester of
Fmoc (Fmoc-NHS) (see Figure 7) reacts with the terminal amine groups of
the surface-bound MUAM molecules to form a carbamate linkage that
covalently attaches the hydrophobic Fmoc group to the surface.

3. Squares of MUAM/Fmoc are removed with ultraviolet (UV)
   photopatterning to create a surface containing squares of bare gold
   surrounded by a hydrophobic background of MUAM/Fmoc.

4. The surface is immersed in a solution of MUAM whereby the bare gold
   areas are filled in with MUAM and remain surrounded by the hydrophobic
   MUAM/Fmoc background.

Figure 7   Surface reaction scheme showing the steps involved in the reversible modifica-
tion of the array background. (*Step 2*) The starting amine-terminated alkanethiol surface
[11-mercaptoundecylamine (MUAM)] is reacted with the reversible protecting group of the
N-hydroxysuccinimide ester of Fmoc (Fmoc-NHS) to create a hydrophobic Fmoc-
terminated surface. (*Step 6*) After DNA immobilization (see Figure 8), the hydrophobic
Fmoc group is removed from the surface using a basic secondary amine, resulting in the
return of the original MUAM surface. (*Step 7*) In the final fabrication step, the deprotected
MUAM is reacted with the NHS ester of methoxypoly(ethylene glycol) propionic acid
(PEG-NHS) to form a PEG-terminated surface that acts to resist the nonspecific binding of
proteins. (Reprinted with permission from Reference 29.)
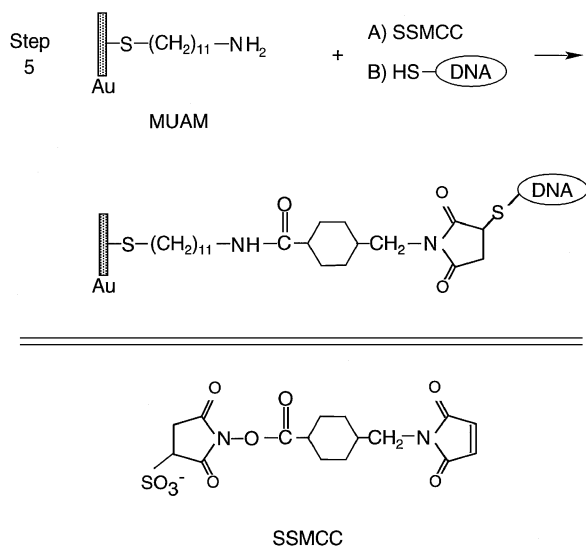
Figure 8   Surface reaction scheme showing the immobilization of thiol-terminated DNA to the array surface. In *Step 5* of the DNA array fabrication, the heterobifunctional linker sulfosuccinimidyl 4-(*N*-maleimidomethyl)cyclohexane-1-carboxylate (SSMCC) is used to attach 5′-thiol–modified oligonucleotide sequences to the reactive 11-mercaptoundecylamine (MUAM) pads. This linker contains an *N*-hydroxysulfosuccinimide (NHSS) ester moiety (reactive toward amines) and a maleimide moiety (reactive toward thiols). (Reprinted with permission from Reference 29.)

5. Single-stranded, thiol-modified DNA sequences are then covalently attached to the MUAM squares using a bifunctional linker (26, 66, 67) and are confined to their respective array locations by the hydrophobic background. The heterobifunctional linker sulfosuccinimidyl 4-(*N*-maleimidomethyl)cyclohexane-1-carboxylate (SSMCC) (see Figure 8) is used to attach 5′ thiol-modified oligonucleotide sequences to the amine-terminated MUAM squares. The linker contains an N-hydroxysulfosuccinimide ester (NHSS) ester functionality (reactive toward amines) and a maleimide functionality (reactive toward thiols).

6. The Fmoc is cleaved from the background using a basic secondary amine, regenerating the original MUAM surface (see Figure 7).

7. The MUAM background is then reacted with the NHS ester of methoxypoly(ethylene glycol) propionic acid (PEG-NHS) to form a background that resists the nonspecific binding of proteins. Specifically, PEG-NHS (see Figure 7) reacts with the deprotected MUAM to form an amide bond that covalently attaches PEG to the array surface.

Explicit details of the above procedure are outlined elsewhere (29).

This procedure is just one of a number of possible methods for the construction of biomolecular arrays on gold thin films. UV photopatterning could easily be substituted by combinations of microcontact printing (68) and self-assembly. Robotics and ink jet printer technology (63, 68) could easily replace the manual delivery of solutions to distinct array locations. Multi-channel flow cells have also been implemented in the fabrication of small-scale arrays (25). On-chip fabrication methods for forming oligonucleotide arrays that are similar to those employed by Affymetrix Inc (Santa Clara, CA) on glass surfaces (69, 70, 71) may also be possible on gold films if the photolabile protection chemistry is compatible with alkanethiol monolayers.

In addition, many other surface chemical attachment schemes can be employed in addition to the maleimide/thiol-modified DNA coupling reaction. Thiol-modified DNA sequences have been attached directly to the gold surface via a gold-thiol bond (7, 72), and many chemistries are available that could link biomolecules to self-assembled films of ω-terminated alkanethiols other than MUAM (26, 27, 73). Also, the site-specific attachment of biotinylated probe molecules to avidin or streptavidin-functionalized gold surfaces has been used as a lower-surface-density attachment method.

APPLICATIONS

The first applications of SPR microscopy involved the imaging of biomolecular surface structures (17), and since then, SPR imaging has been used in many surface morphological investigations. For example, Evans et al (19) employed SPR imaging to monitor the growth of self-assembled multilayer structures on predefined templates. Here, a dual-component monolayer sample [C18-thiol vs COOH-$(CH_2)_{15}$-SH] was prepared by stamping methods. The sample was then immersed in an aqueous solution of copper acetate whereby Cu ions adsorbed at the acid-functionalized sites on the sample surface. Subsequent layers of alkanethiol could then be adsorbed to the surface by means of this charged bridging group. SPR imaging was used both as a measure of film thickness and as a test of film homogeneity. Duschl et al (21) have used the SPR imaging technique to characterize supported lipid bilayer films engineered to mimic cell membranes and to support the reconstitution of transmembrane proteins. In a similar vein, Florin & Gaub (74) investigated the electrical and mechanical properties of supported lipid films, termed painted supported membranes, using SPR imaging methods. SPR microscopy has also been used to observe the cell/substrate contact distances of living cells contained in cultures (75).

Because of its surface-sensitive nature, SPR imaging provides a valuable tool for the study of thin polymer films at metal interfaces, and it has been applied in optical storage experiments involving liquid crystalline polymer thin films (20). Evans et al (76) used SPR microscopy to characterize spatially the anchoring of adsorbed nematic liquid crystalline films at derivatized self-assembled monolayer

surfaces; their results show that the technique is sensitive to the alignment of molecules within ∼300 nm of the surface. Additionally, phase changes induced in the polymer film on heating or cooling were tracked by SPR imaging through changes in film refractive index. Sawodny et al (77) employed SP optical techniques (including imaging) to characterize the optical and structural properties of thin films of poly(methyl-phenyl-silane). Exposure to deep UV irradiation caused photovolatilization of these films; conditions under which such film ablation (or etching) occurred were pinpointed using data extracted from SPR images.

SPR imaging has also been employed successfully in a number of biomolecular recognition applications. The specific binding of the protein streptavidin to surface bound, self-assembled monolayer films of biotin-functionalized alkanethiols (18) or Langmuir-Blodgett–transferred films of biotinylated phospholipids (78, 79) has been monitored using SPR microscopy. Similarly, the technique has been employed in the investigation of the site-selective binding of the antigen hapten to a surface patterned with lipid-anchored antibody binding sites (24). In numerous demonstrations (26–28, 80), SPR imaging has been shown to be effective in the study of oligonucleotide hybridization events, and the technique could potentially serve as the basis for the development of massive on-line hybridization-adsorption assays. Recent focus in our own laboratory involves the use of SPR imaging detection for the monitoring of sequence-specific protein-DNA interactions, and data from two ongoing projects is presented in the following sections.

Single-Stranded DNA Binding Protein

Single-stranded DNA binding protein (SSB) (a tetramer of four identical subunits with a total molecular weight of 75,000) binds tightly and selectively to single-stranded DNA sequences (81). SSB serves an important function in DNA replication, repair, and recombination through its ability to prevent the premature reannealing of complementary DNA sequences. The binding of SSB to surface-immobilized, single-stranded DNA sequences has been monitored previously using the BIAcore scanning angle instrument (10). SPR imaging measurements, when combined with the array fabrication techniques discussed earlier, can be used to successfully monitor the simultaneous binding of the SSB protein to arrays of bound oligonucleotide sequences.

Figure 9 shows four in situ SPR images of a DNA array that has been exposed to a series of aqueous solutions containing either a complementary DNA sequence or the protein SSB. A checkerboard array of 750-μm suqares containing two 16-base, noninteracting DNA sequences (referred to here as probes A and B) was fabricated. Figure 9a depicts the difference between two images taken immediately before and after the exposure of this array to a solution containing the complementary sequence to only surface-bound probe A. The raised areas on the image represent changes in %R on hybridization-adsorption (formation of double-stranded DNA) at locations with immobilized probe A. The array was subsequently exposed to a 100 nM solution of single-stranded DNA binding protein;
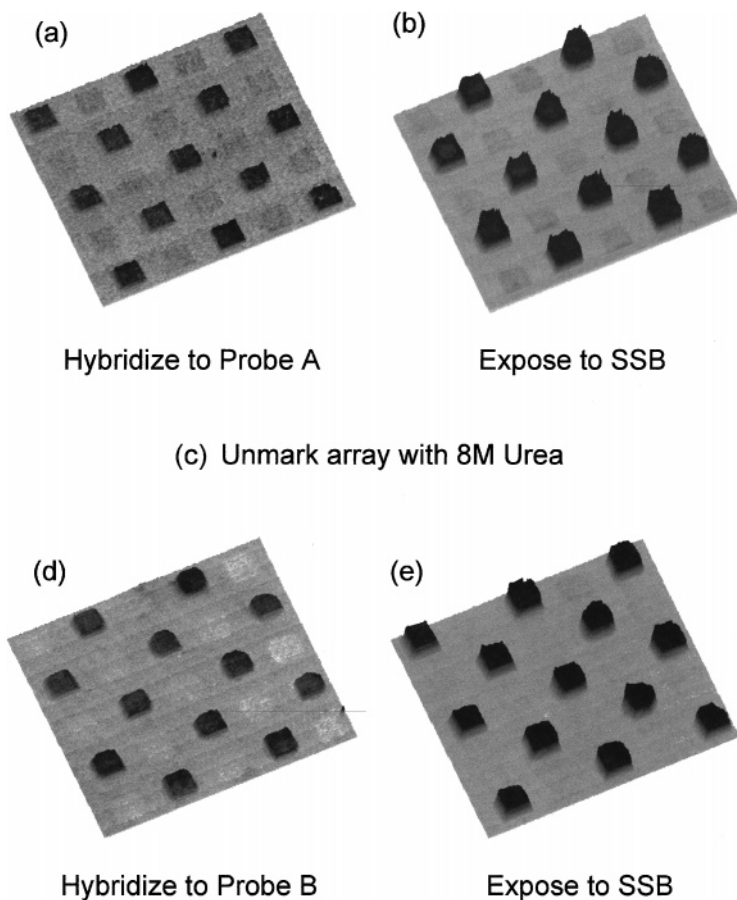
Figure 9   Surface plasmon resonance difference images of single-stranded DNA binding protein (SSB) adsorption onto a photopatterned DNA array. A dual-component DNA array was created with 16-mer probes A and B immobilized in a checkerboard pattern. (*a*) The difference between two in situ images collected immediately before and after exposure of the array to a solution containing the complementary sequence to probe A only. The raised spots indicate an increase in the percentage of reflectivity due to DNA duplex formation. (*b*) Difference image showing the effects of exposing the surface to a 100 nM solution of the protein SSB. The protein binds only at probe B, which contains single-stranded DNA. (*c*) The array is regenerated in an "unmarking" step during which the surface is soaked in 8 M urea. (*d*) Difference image showing the effects of exposing the same array surface to a solution containing the complementary sequence to DNA probe B. (*e*) Difference image collected after exposure of the surface to SSB.

the difference image generated during this step is shown in Figure 9*b*. Note the increase in signal at array locations opposite those that increased during the previous step. These locations contained DNA probe B, which remained single-stranded. No increase in signal was observed at the double-stranded, probe A locations, indicating that the SSB protein bound specifically to the single-stranded DNA sequences and did not adsorb nonspecifically to the poly(ethylene glycol)-modified array background.

A second set of experiments on the same surface was used to demonstrate the reversibility of DNA hybridization and SSB binding and the reusability of the DNA arrays. The surface was exposed to a solution of 8 M urea for 20 min and subsequently rinsed with water in an "unmarking" step. This process denatures the SSB protein and disrupts the hydrogen bonding in the DNA duplex in order to regenerate the original single-stranded DNA surface. Complete regeneration of the surface was verified by comparing the appropriate images (data not shown). The reusability of the single-stranded DNA array was then investigated by exposing the surface to a solution that this time contained DNA complementary to probe B. The resulting difference image (Figure 9*d*) shows an increase in binding at location B due to hybridization-adsorption. In the final step, the array was again exposed to a solution of SSB. The protein bound at locations containing probe A (see Figure 9*e*), which this time remained single-stranded but not at locations containing double-stranded probe B.

It is important to note that the increase in signal on protein binding is significantly more intense than that seen on mere hybridization adsorption. This is due not to a greater number of binding events but to the much larger size of the protein in comparison with a 16-mer DNA sequence. In actuality, a far greater number of binding events is expected between the complementary DNA sequences than between the single-stranded probes and the protein (due to steric hindrance). A more detailed quantitative analysis of the efficiencies of binding of both the complementary DNA sequences and the SSB protein is forthcoming (82).

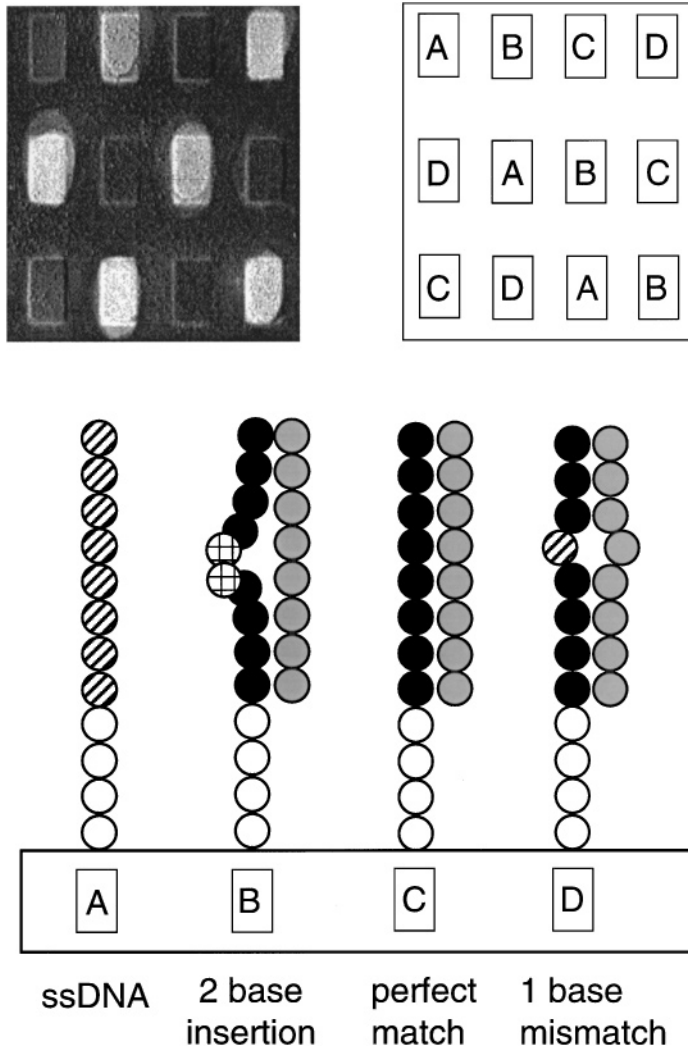## *Escherichia coli* Mismatch Binding Protein

Mismatch binding proteins such as that of *E. coli* (MutS) are used by biological systems to help detect and repair replication errors in genomic DNA. The ability of these proteins to identify single-base mismatches and short insertions and deletions in double-stranded DNA has led to the application of mismatch proteins in mutation and single nucleotide polymorphism detection assays (83–86). In addition, the recent discovery of a link between the malfunction of postreplication mismatch correction and hereditary nonpolyposis colorectal cancer has renewed interest in these repair systems (87). In a second example of the application of SPR imaging techniques to the in situ study of protein adsorption onto immobilized DNA arrays (23, 29), we demonstrate that SPR imaging measurements can be used as a rapid and efficient method for screening the sequence-specific binding of the protein MutS to mismatched DNA.

Previous researchers have used a variety of methods to study the binding of MutS to double-stranded DNA, including nitrocellulose filter binding assays, nuclease protection assays, and band shift assays (88). None of these methods is ideal because either they perturb the protein during filter immobilization or they measure the protein-DNA binding only indirectly. In contrast, SPR techniques are well suited to the direct monitoring of these reversible, protein-DNA interactions. Although the commercial BIAcore SPR instrument has been used previously to study the interaction of MutS with DNA molecules incorporated into thin dextran films (8, 11), SPR imaging is more ideally suited to the problem because the in situ binding of the MutS protein to large numbers of surface-bound oligonucleotide sequences can be monitored simultaneously.

Figure 10 shows an in situ SPR image of a DNA array onto which the protein MutS has been adsorbed. Four different 30-mer DNA molecules (labeled A–D) were attached to a gold surface whose background was modified in such a way as to resist the nonspecific adsorption of proteins. (Details concerning the preparation of such DNA arrays are outlined above.) The surface in Figure 10 was first exposed to a solution containing the sequence C*. This oligonucleotide (*a*) does not bind at all to probe A, leaving it single stranded (ssDNA), (*b*) binds to probe B to create a DNA duplex with a two base insertion (2bi), (*c*) binds to probe C to create a perfectly complementary DNA duplex (perfect match), and (*d*) binds to probe D to create a DNA duplex with a single-base mismatch (sbm). The surface was then exposed to a 200 nM solution of MutS. As seen in Figure 10, a substantial amount of protein binding occurred to the sbm and 2bi array locations, and no significant MutS binding was observed for the perfectly matched and ssDNA.

The adsorption of MutS onto these DNA sequences is quantified more precisely by line profiles (shown in Figure 11) taken through four spots on the array. These line profiles plot changes in the percent reflectivity (%R) as a function of array position and were measured for the starting probe surface, the surface after exposure to complementary DNA sequences, and the surface after exposure to MutS. As seen in Figure 11*A*, the amount of adsorption of the complementary 30-mer sequence is equivalent for the perfect match, 2bi, and sbm and is nonexistent for the ssDNA probe spot. The profile corresponding to the binding of MutS shows that there is no detectable protein adsorption onto the ssDNA and perfect match spots; this is different from previous results obtained for DNA molecules that had been incorporated into dextran polymer films (8, 11). From previous experiments (26), we estimate a surface density of 10^{13} molecules/cm^2 for the DNA probes, which corresponds to approximately 100 fmol of DNA per $750 \times 750 \ \mu$m array spot. At this surface density, there appears to be sufficient room for the specific binding of the 97-kDa MutS protein to the surface-bound probes.

For the experiment in Figure 11*a*, the sbm was a G/T mismatch, which is known to have the strongest MutS-DNA binding interaction (89). The adsorption of MutS onto the sbm leads to a large signal increase; the adsorption onto the 2bi gives a similar signal. In Figure 11*B*, the experiment was repeated, replacing the G/T mismatch with an A/C mismatch, which was expected to bind the MutS protein less

Figure 10 Surface plasmon resonance (SPR) imaging measurements of adsorption of the *Escherichia coli* mismatch binding protein (MutS) onto DNA arrays. An array was created with DNA probes A–D immobilized in the pattern depicted in the *upper right* portion of the figure. The array was then exposed to a solution containing the sequence C*. This oligonucleotide (*a*) does not bind at all to probe A, leaving it single stranded (ssDNA), (*b*) binds to probe B to create a duplex containing a two-base insertion, (*c*) binds to probe C in a perfectly complementary manner, and (*d*) binds to probe D to form a duplex containing a single-base mismatch. The *upper left* portion of the figure shows an SPR difference image of the binding of MutS to the array. The image shown is a difference between two images collected before and after exposure of the surface to MutS.
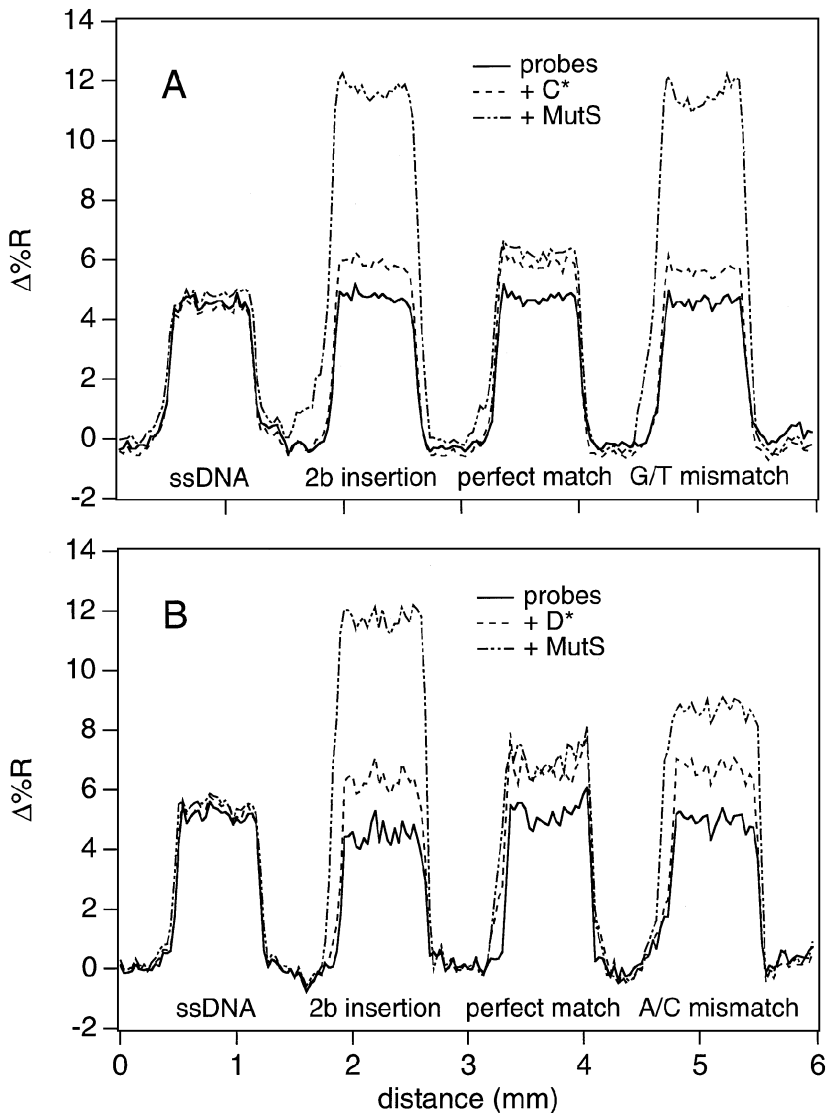
Figure 11 Line profiles showing in situ hybridization and the adsorption of *Escherichia coli* mismatch binding protein (MutS) onto DNA arrays containing oligonucleotide sequences A–D. (*A*) The *solid line* is the percent reflectivity (%R) measured for the starting DNA probe surface. The *dashed line* is the %R measured after exposing the surface to a 2 μM solution of the complement C*. This DNA sequence binds not at all to probe A, creates a two-base insertion with B, is a perfect match to C, and creates a G/T mismatch with D. The *dot-dashed line* is the %R measured after exposing the surface to a 200 nM solution of MutS. Measurable protein binding occurred at the array locations that contained the two-base insertion and a G/T mismatch. (*B*) An experiment similar to panel *A* in which an A/C single-base mismatch is formed. The positions of probes C and D have been switched on the array surface (from that depicted in Figure 10) and the surface was exposed to complement D*. The MutS protein again binds at the positions of the two-base insertion and the single-base mismatch. ssDNA, single-stranded DNA.

well (89). (To achieve this, the positions of DNA probes C and D and were reversed and the array was exposed to the complement D^*.) In this case, the binding of MutS to the A/C mismatch is weaker than that seen for the 2bi. DNA array hybridization assays based upon free energy differences cannot discriminate single-base mismatches in sequences longer than approximately 30 bases. Using MutS, such mismatches can easily be identified, and this may provide a powerful new method for the detection and identification of single nucleotide polymorphisms. To determine the potential utility of the protein in mismatch detection assays, the binding of MutS to arrays of double-stranded DNA containing all eight possible mismatches must be measured; these experiments are currently in progress.

CONCLUSIONS

The combined simplicity and versatility of SPR imaging measurements make them ideally suited to the study of ultrathin organic films. The technique is extremely sensitive, provides reasonable lateral resolution, and can be used in both ex situ and in situ configurations to monitor the real-time binding of label-free analyte molecules to metal surfaces. The two-dimensional analysis of imaging data, combined with recently introduced techniques for the fabrication of arrays on gold surfaces, makes SPR imaging a powerful tool for the parallel processing of multiple biomolecular interactions. Although the technique is currently confined to research laboratories, commercialization of an SPR imaging instrument is on the horizon, and this will undoubtedly lead to the routine application of SPR microscopy to any number of biomedical or biotechnical screening assays.

ACKNOWLEDGMENTS

Visit the Annual Reviews home page at www.AnnualReviews.org

LITERATURE CITED

1. Löfås S, Malmqvist M, Rönnberg I, Stenberg E, Liedberg B, Lundström I. 1991. *Sens. Actuators B* 5:79–84
2. Malmqvist M. 1993. *Nature* 361:186–87
3. Rahn JR, Hallock RB. 1995. *Langmuir* 11:650–54
4. Brynda E, Homola J, Houska M, Pfeifer P, Skvor J. 1999. *Sens. Actuators B* 54:132–36
5. Nilsson P, Persson B, Uhlen M, Nygren PA. 1995. *Anal. Biochem.* 224:400–8
6. Bates PJ, Dosanjh HS, Kumar S, Jenkins TC, Laughton CA, Neidle S. 1995. *Nucleic Acids Res.* 23:3627–32
7. Peterlinz KA, Georgiadis RM, Herne TM, Tarlov MJ. 1997. *J. Am. Chem. Soc.* 119: 3401–2

8. Babic I, Andrew SE, Jirik FR. 1996. *Mutat. Res.* 372:87–96

9. Bondeson K, Frostell-Karlsson A, Fagerstam L, Magnusson G. 1993. *Anal. Biochem.* 214:245–51

10. Fisher RJ, Fivash M, Casas-Finet J, Bladen S, McNitt KL. 1994. *Methods Companion Methods Enzymol.* 6:121–33

11. Gotoh M, Hasebe M, Ohira T, Hasegawa Y, Shinohara Y, et al. 1997. *Genet. Anal. Biomol. Eng.* 14:47–50

12. Silin V, Plant A. 1997. *Trends Biotechnol.* 15:353–59

13. Fivash M, Towler EM, Fisher RJ. 1998. *Curr. Opin. Biotechnol.* 9:97–101

14. Yeatman E, Ash EA. 1987. *Electron. Lett.* 23:1091–92

15. Yeatman E, Ash EA. 1988. *SPIE Scanning Microsc. Technol. Appl.* 897:100–7

16. Rothenhausler B, Knoll W. 1988. *Nature* 332:615–17

17. Hickel W, Kamp D, Knoll W. 1989. *Nature* 339:186

18. Haussling L, Ringsdorf H, Schmitt F-J, Knoll W. 1991. *Langmuir* 7:1837–40

19. Evans SD, Flynn TM, Ulman A. 1995. *Langmuir* 11:3811–14

20. Hickel W, Knoll W. 1990. *Thin Solid Films* 187:349–56

21. Duschl C, Liley M, Lang H, Ghandi A, Zakeeruddin SM, et al. 1996. *Mater. Sci. Eng. C* 4:7–18

22. Jordan CE, Corn RM. 1997. *Anal. Chem.* 69:1449–56

23. Nelson BP, Frutos AG, Brockman JM, Corn RM. 1999. *Anal. Chem.* 71:3928–34

24. Fischer B, Heyn SP, Egger M, Gaub HE. 1993. *Langmuir* 9:136–40

25. Berger CEH, Beumer TAM, Kooyman RPH, Greve J. 1998. *Anal. Chem.* 70:703–6

26. Jordan CE, Frutos AG, Thiel AJ, Corn RM. 1997. *Anal. Chem.* 69:4939–47

27. Thiel AJ, Frutos AG, Jordan CE, Corn RM, Smith LM. 1997. *Anal. Chem.* 69:4948–56

28. Frutos AG, Corn RM. 1998. *Anal. Chem.* 70:A449–55

29. Brockman JM, Frutos AG, Corn RM. 1999. *J. Am. Chem. Soc.* 121:8044–51

30. Kano H, Kawata S. 1996. *Opt. Lett.* 21:1848–50

31. Knobloch H, Brunner H, Leitner A, Ausseneg F, Knoll W. 1993. *J. Chem. Phys.* 98:10093–95

32. Corn RM, Philpott MR. 1984. *J. Chem. Phys.* 80:5245–49

33. Knobloch H, Duschl C, Knoll W. 1989. *J. Chem. Phys.* 91:3810–14

34. Knoll W, Philott MR, Swalen JD, Girlando A. 1982. *J. Chem. Phys.* 77:2254–60

35. Simon HJ, Benner RE, Rako JG. 1977. *Opt. Commun.* 23:245

36. Corn RM, Romagnoli M, Levenson MD, Philpott MR. 1984. *Chem. Phys. Lett.* 106:30–35

37. Hanken DG, Jordan CE, Frey BL, Corn RM. 1998. *Electroanal. Chem.* 20:141–225

38. Knoll W. 1998. *Annu. Rev. Phys. Chem.* 49:569–638

39. Hansen WN. 1968. *J. Opt. Soc. Am.* 58:380

40. Kaschke S. 1995. *Schott '96 for Windows Catalog Optical G/95S,* Version 1.1. Mainz, Ger.: Schott Glasswerke

41. Johnson PB, Christy RW. 1972. *Phys. Rev. B* 6:4370–79

42. Thormahlen I, Straub J, Grigull U. 1985. *J. Phys. Chem. Ref. Data* 14:933–45

43. Campbell DJ. 1990. *Second harmonic generation studies of chemisorption at electrode surfaces.* PhD thesis. Univ. Wis., Madison. 347 pp.

44. Peterlinz KA, Georgiadis R. 1996. *Opt. Commun.* 130:260–66

45. Bradberry GW, Sambles JR. 1988. *Opt. Commun.* 67:404–8

46. Yang FZ, Bradberry GW, Jarvis DJ, Sambles JR. 1990. *J. Mod. Opt.* 37:977–91

47. Yang FZ, Bradberry GW, Sambles JR. 1990. *J. Mod. Opt.* 37:993–1003

48. Brink G, Sigl H, Sackmann E. 1995. *Sens. Actuators B* 24/25:751–56

49. Melendez J, Carr R, Bartholomew D, Taneja H, Yee S, et al. 1997. *Sens. Actuators B* 38/39:375–79

50. Zhang LM, Uttamchandani D. 1988. *Electron. Lett.* 24:1469–70

51. Tubb AJC, Payne FP, Millington RB, Lowe CR. 1997. *Sens. Actuators B* 41:71–79

52. Jory MJ, Vukusic PS, Samples JR. 1994. *Sens. Actuators B* 17:203–9

53. Aldinger U, Pfeifer P, Schwotzer G, Steinrucke P. 1998. *Sens. Actuators B* 51:298–304

54. Homola J. 1997. *Sens. Actuators B* 41:207–11

55. Hanning A, Roeraade J, Delrow JJ, Jorgenson RC. 1999. *Sens. Actuators B* 54:25–36

56. Johnston KS, Mar M, Yee SS. 1999. *Sens. Actuators B* 54:57–65

57. Stemmler I, Brecht A, Gauglitz B. 1999. *Sens. Actuators B* 54:98–105

58. Frutos AG, Weibel SC, Corn RM. 1999. *Anal. Chem.* 71:3935–40

59. Knobloch H, von Szada-Borryszkowski G, Woigk S, Helms A, Brehmer L. 1996. *Appl. Phys. Lett.* 69:2336–37

60. Berger CEH, Kooyman RPH, Greve J. 1994. *Rev. Sci. Instrum.* 65:2829–36

61. Yeatman EM. 1996. *Biosens. Bioelectron.* 11:635–49

62. Kooyman RPH, Krull UJ. 1991. *Langmuir* 7:1506–9

63. Zizlsperger M, Knoll W. 1998. *Progr. Colloid Polym. Sci.* 109:244–53

64. Frutos AG, Brockman JM, Corn RM. 2000. *Langmuir.* 16:2192–97

65. Atherton E, Sheppard RC. 1989. *Solid Phase Peptide Synthesis: A Practical Approach*. Oxford, UK: IRL. 203 pp.

66. Frey BL, Corn RM. 1996. *Anal. Chem.* 68:3187–93

67. Frutos AG, Liu Q, Thiel AJ, Sanner AMW, Condon AE, et al. 1997. *Nucleic Acids Res.* 25:4748–57

68. Kumar A, Abbott NL, Kim E, Biebuyck HA, Whitesides GM. 1995. *Acc. Chem. Res.* 28:219–26

69. Fodo SPA, Read JL, Pirrung MC, Stryer L, Tsai LA, Solas D. 1991. *Science* 251:767–73

70. Pease AC, Solas D, Sullivan EJ, Cronin MT, Holmes CP, Fodor SPA. 1994. *Proc. Natl. Acad. Sci. USA* 91:5022–26

71. Singh-Gasson S, Green RD, Yue Y, Nelson C, Blattner F, et al. 1999. *Nat. Biotech.* 17:974–78

72. Herne TM, Tarlov MJ. 1997. *J. Am. Chem. Soc.* 119:8916–20

73. Boncheva M, Scheibler L, Lincoln P, Vogel H, Akerman B. 1999. *Langmuir* 15:4317–20

74. Florin E-L, Gaub HE. 1993. *Biophys. J.* 64:375–83

75. Giebel K-F, Bechinger C, Heminghaus S, Riedel M, Leiderer P, et al. 1999. *Biophys. J.* 76:509–16

76. Evans SD, Allinson H, Boden N, Flynn TM, Henderson JR. 1997. *J. Phys. Chem. B* 101:2143–48

77. Sawodny M, Stumpe J, Knoll W. 1991. *J. Appl. Phys.* 69:1927–35

78. Schmitt F-J, Knoll W. 1991. *Biophys. J.* 60:716–20

79. Schmitt F-J, Weisenhorn AL, Hansma PK, Knoll W. 1992. *Thin Solid Films* 210/211:666–69

80. Piscevic D, Lawall R, Veith M, Liley M, Okahata Y, Knoll W. 1995. *Appl. Surf. Sci.* 90:425–36

81. Meyer RR, Laine PS. 1990. *Microbiol. Rev.* 54:342–80

82. Nelson BP, Corn RM. Manuscript in preparation

83. Ellis LA, Taylor GR, Banks R, Baumberg S. 1994. *Nucleic Acids Res.* 22:2710–11

84. Lishanski A, Ostrander EA, Rine J. 1994. *Proc. Natl. Acad. Sci. USA* 91:2674–78

85. Wagner R, Debbie P, Radman M. 1995. *Nucleic Acids Res.* 23:3944–48

86. Bellanne-Chantelot C, Feaufils S, Hourdel V, Lesage S, Morel V, et al. 1997. *Mutat. Res. Genom.* 382:35–43

87. Jirincy J. 1998. *EMBO J.* 17:6427–36

88. Wagner R, Radman M. 1995. *Methods Companion Methods Enzymol.* 7:199–203

89. Su SS, Lahue RS, Au KG, Modrich P. 1987. *J. Biol. Chem.* 263:6829–35